

**Pursuing Reliable Thermal Analysis Techniques for Energetic Materials:
Decomposition Kinetics and Thermal Stability of Dihydroxylammonium 5,5'-
Bistetrazole-1,1'-Diolate (TKX-50)**

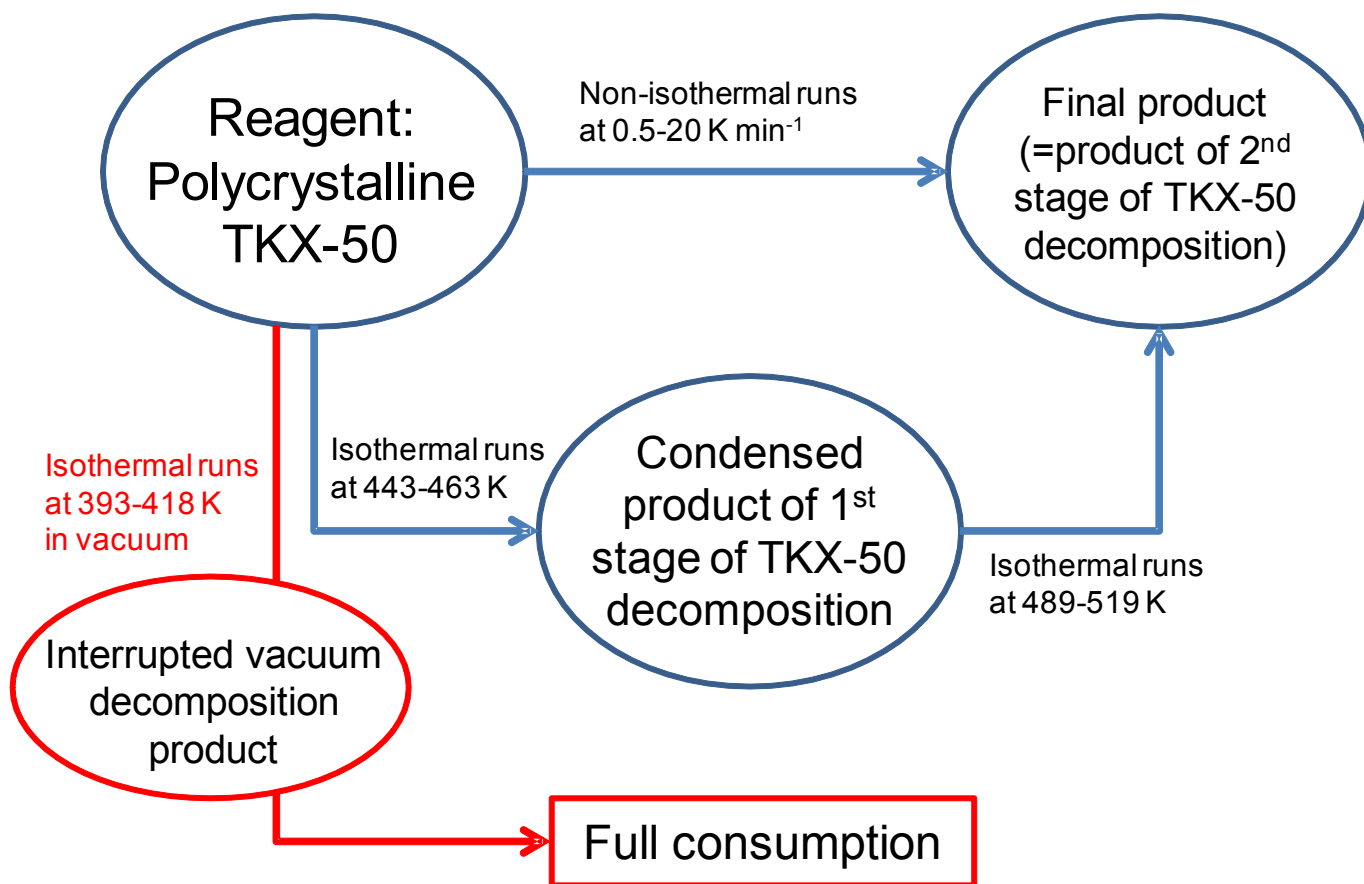
*Nikita V. Muravyev, Konstantin A. Monogarov, Andrey F. Asachenko, Mikhail S. Nechaev,
Ivan V. Ananyev, Igor V. Fomenkov, Vitaly G. Kiselev, and Alla N. Pivkina*

ELECTRONIC SUPPORTING INFORMATION

Contents

1. Logical Scheme of the Study	S2
2. Characterization of Condensed Decomposition Products of TKX-50	S3
3. Scanning Electron Microscopy Images of Pristine TKX-50 and Condensed Products of Thermolysis.....	S6
4. Kinetics of TKX-50 decomposition: Raw thermoanalytical data and models employed S8	
5. Analysis of the evolved gases by IR spectroscopy	S17
6. Accelerating rate calorimetry: experiment and modeling.....	S18
7. Recommended kinetic parameters for first stage of TKX-50 decomposition	S20

1. Logical Scheme of the Study



Scheme S1. The interplay of the thermoanalytical experiments employed in the present work under normal pressure (blue) and vacuum (red).

2. Characterization of Condensed Decomposition Products Of TKX-50

Condensed product of the 1st stage of decomposition (ABTOX)

Brown solid powder

¹³C NMR ([D₆]-DMSO, 25 °C): $\delta = 134.4$ (CN₄O) ppm. Literature data for ABTOX [a]: 134.8 ppm.

MS (FAB⁻): $m/z = 169.0$ [C₂N₈O₂⁻];

IR (KBr): $\nu = 3183$ (w), 3049 (w), 2858 (w), 2343 (w), 2277 (w), 2153 (w), 2002 (w), 1967 (w), 1832 (w), 1687 (w), 1671 (m), 1500 (w), 1432 (m), 1421 (s), 1353 (s), 1278 (w), 1232 (vs), 1165 (vs), 1048 (vs), 998 (vs), 881 (w), 729 (vs), 677 (w), 502 (vs) cm⁻¹.

Elemental analysis: found C 13.11, H 3.34, N 68.58. Literature data for ABTOX [a]: found C 12.14, H 3.69, N 68.18. Calculated for ABTOX (C₂H₈N₁₀O₂): C 11.77, H 3.95, N 68.61.

The recrystallization of the powder from water at room temperature led to the precipitation of prismatic colorless crystals. Ten random crystals were chosen for X-ray diffraction (XRD) study. The XRD indexing of unit cell parameters were carried out using a Bruker APEX II CCD diffractometer (MoK α radiation, graphite monochromator, ω -scans) and software packages APEX 2 [b] and CELL_NOW [c]. Indexing of each crystal yielded unit cell parameters $a = b \approx 7.5$ Å, $c \approx 13.3$ Å, $\alpha = \beta = \gamma \approx 90^\circ$, which were close to those observed previously for crystals of the ammonium salt of 5,5'-bis-tetrazole-1-oxide (ABTOX) [a] and reported in the Cambridge Structural Database [d]. For one of ABTOX crystals the full routine XRD study was performed in order to unambiguously confirm its structure.

The crystal of ABTOX (C₂H₈N₁₀O₂, M = 204.18) is orthorhombic, space group I222, at 120K: $a = b = 7.5084(10)$, $c = 13.3166(19)$, $V = 750.38(18)$ Å³, $Z = 4$ ($Z' = 0.5$), $d_{\text{calc}} = 1.807$ gcm⁻³, $\mu(\text{MoK}\alpha) = 0.90$ cm⁻¹, $F(000) = 424$. Intensities of 4337 reflections were measured with a Bruker APEX II CCD diffractometer [$\lambda(\text{MoK}\alpha) = 0.71072$ Å, ω -scans, $2\theta < 61^\circ$], and 1173 independent reflections [$R_{\text{int}} = 0.0625$] were used in further refinement. The structure (Figure S1) was solved by direct method and refined by the full-matrix least-squares technique against F^2 in the isotropic approximation. The anion moiety is translationally and positionally disordered (Figure S2) as it has been previously reported [a]; hence, the refinement succeeds if only all atoms are refined in the isotropic approximation. All attempts to find any twin law (using CELL_NOW and PLATON programs) or less symmetrical structure solution failed. Hydrogen atoms were found in difference Fourier synthesis and were refined in the riding model. For

ABTOX, the refinement converged to $wR2 = 0.1948$ for all independent reflections ($R1 = 0.0723$ was calculated against F for 996 observed reflections with $I > 2\sigma(I)$). All calculations were performed using SHELXTL 2014. [e]. Since the structure of ABTOX has been reported [a], we do not show the full set of geometric parameters.

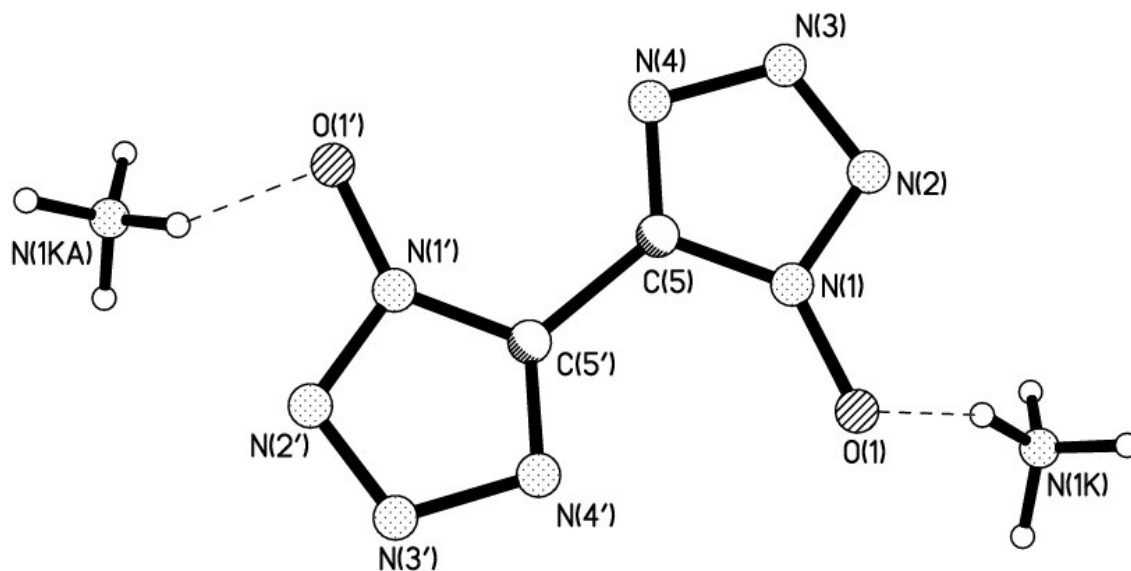


Figure S1. The general view of the ABTOX salt in crystal. The dashed lines denote some NH...O hydrogen bonds.

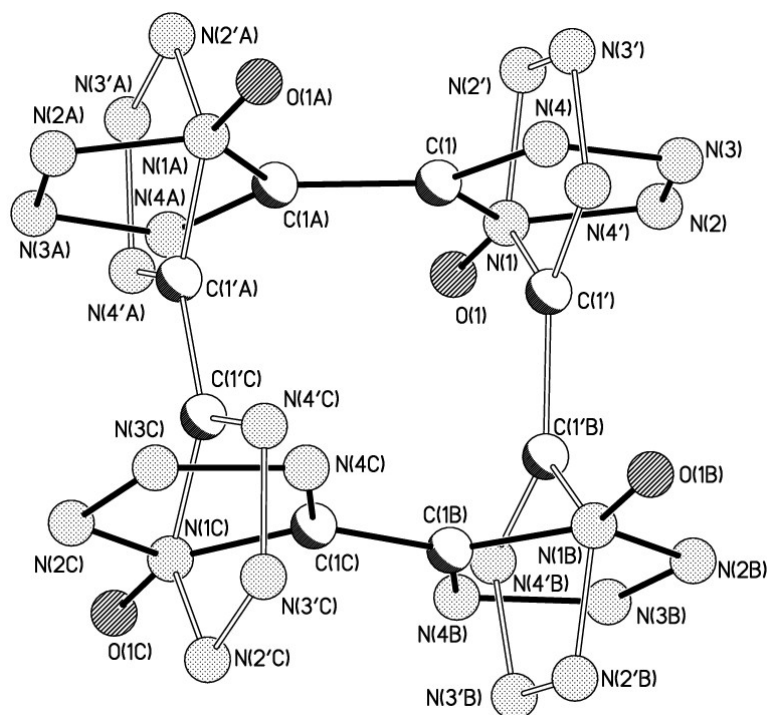


Figure S2. Disorder of the anion moiety in the crystal structure of ABTOX.

Interrupted vacuum decomposition product (VP)

White solid powder

Stoichiometry approx. 10% TKX-50 + 90% BTO

IR (KBr): $\nu = 3128$ (w), 3057 (w), 2980 (w), 2890 (w), 1781 (w), 1577 (w), 1524 (w), 1479 (w), 1412 (s), 1376 (s), 1273 (vs), 1236 (m), 1196 (vs), 1121 (vs), 1044 (m), 1010 (vs), 800 (s), 707 (w), 654 (vs), 499 (m), 453 (m) cm^{-1} .

Elemental analysis: found C 13.25, H 1.59, N 65.03.

Final decomposition product (FP)

Black solid powder

Stoichiometry [C₅H₅N₈O]

IR (KBr): $\nu = 3213$ (w), 3088 (w), 2346 (w), 1703 (vs), 1638 (m), 1527 (w), 1391 (s), 1195 (w), 1122 (m), 975 (m), 789 (s), 764 (m), 689 (w), 520 (m), 457 (s) cm^{-1} .

Elemental analysis: found C 31.15, H 2.52, N 57.38.

[a] Fischer, N.; Klapotke, T. M.; Reymann, M.; Stierstorfer, J., Nitrogen-Rich Salts of 1H,1H-5,5-Bitetrazole-1,1-diol: Energetic Materials with High Thermal Stability. *Eur. J. Inorg. Chem.* **2013**, 2167-2180.

[b] APEX 2, version 1.0-22, Bruker (2004), Bruker AXS Inc., Madison, Wisconsin, USA.

[c] CELL_NOW, version 12-31-03, Bruker (2003), Bruker AXS Inc., Madison, Wisconsin, USA.

[d] Taylor, R.; Allen, F. H., Statistical and Numerical Methods of Data Analysis, in Structure Correlation, Volume 1 (Eds Bürgi H.-B.; Dunitz J. D.), 1994, Wiley-VCH Verlag GmbH, Weinheim, Germany.

[e] Sheldrick, G.M., A short history of SHELX. *Acta Crystallogr.* 2008, A64(1), 112-122.

3. Scanning Electron Microscopy Images of Pristine TKX-50 and Condensed Products of Thermolysis

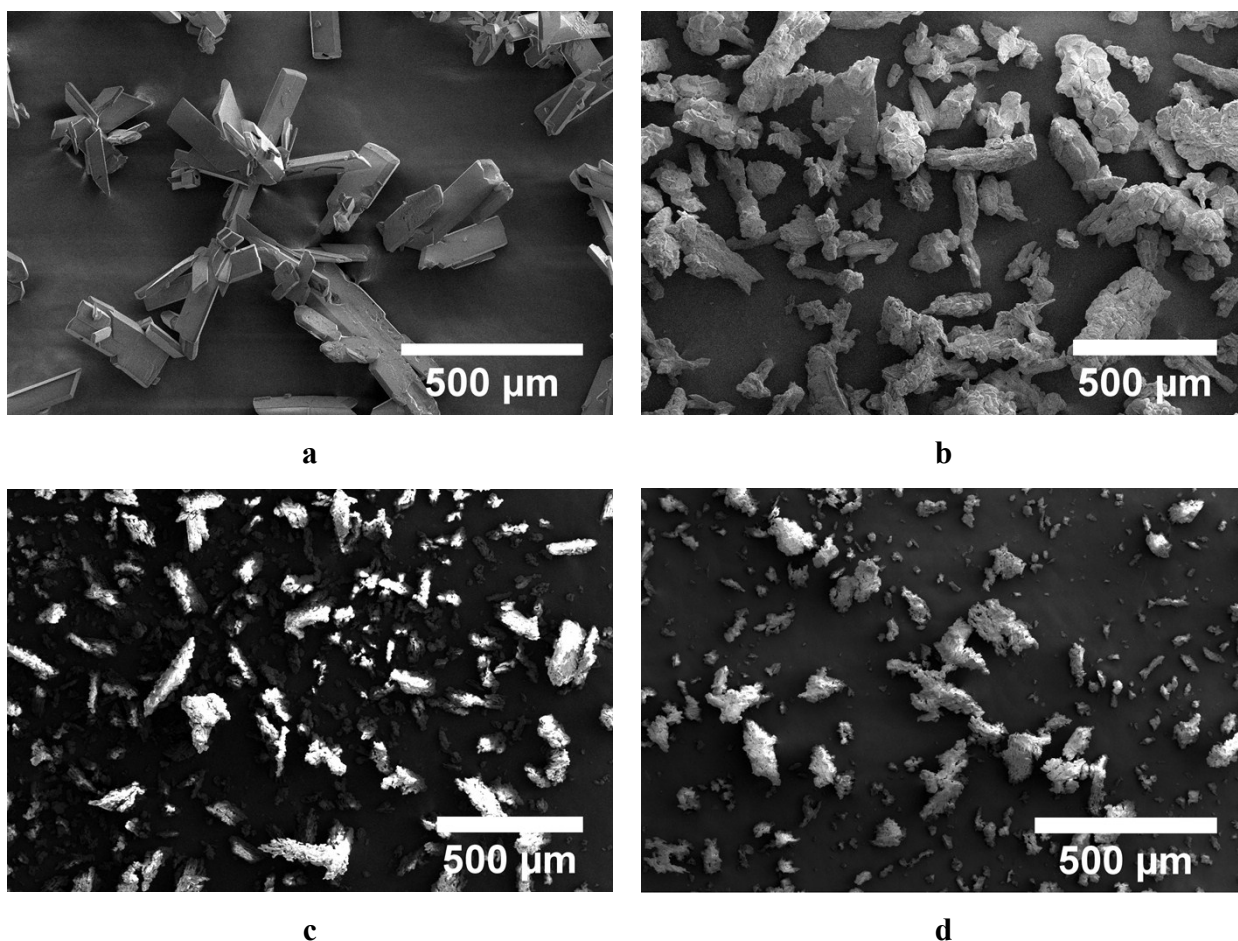
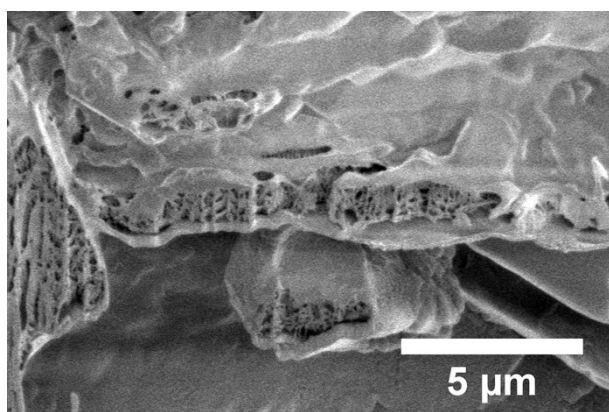
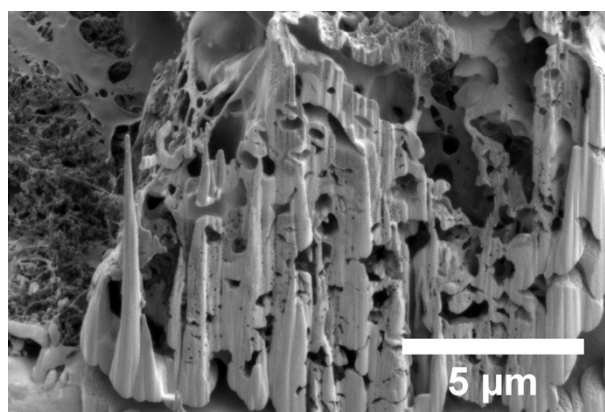


Figure S3. Scanning electron microscopy images of the condensed materials studied: (a) pristine TKX-50 powder; (b) solid product of interrupted vacuum decomposition of TKX-50 (VP); (c) solid product of the isothermal ageing of TKX-50 (SP); (d) final TKX-50 decomposition condensed product (FP).



SP



FP

Figure S4. Scanning electron microscopy images of the solid products SP (Figure S3(c)) and FP (Figure S3(d)): particles cut with focused ion beam in scanning electron microscopy (SEM). The highly porous internal structure of the SP sample is evident.

4. Kinetics of TKX-50 decomposition: Raw thermoanalytical data and models employed

4a. Raw Non-Isothermal DSC data of TKX-50 Decomposition: Two-stage Thermolysis

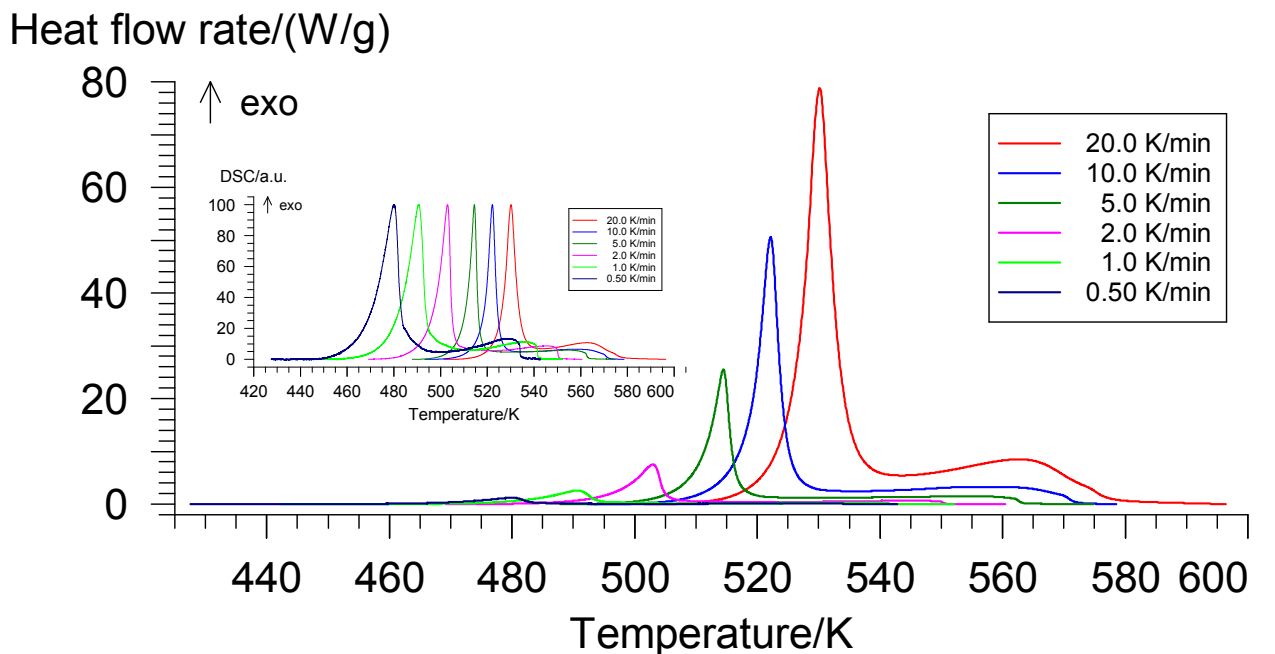


Figure S5. DSC curves of TKX-50 samples at heating rates of 0.5-20 K min⁻¹ and sample mass of 1 mg. These values correspond to the datasets #1 and 2 in Table 1. The inset represents the normalized DSC data.

Note that we cannot use kinetic deconvolution techniques (i.e., representation of the overall complex process as the sum of the independent stages) for our consecutive processes observed in non-isothermal runs (Figure S5). To explain rationales for this fact, let us consider the simple model comprised of the two first-order reactions. The conversion degrees are

$$\frac{d\alpha_1}{dt} = A_1 e^{-E_{a1}/(RT)} \cdot (1 - \alpha_1), \quad \frac{d\alpha_2}{dt} = A_2 e^{-E_{a2}/(RT)} \cdot (\alpha_1 - \alpha_2),$$

and the overall conversion degree is:

$$\frac{d\alpha}{dt} = \eta \frac{d\alpha_1}{dt} + (1 - \eta) \frac{d\alpha_2}{dt} = \eta A_1 e^{-E_{a1}/(RT)} \cdot (1 - \alpha_1) + (1 - \eta) A_2 e^{-E_{a2}/(RT)} \cdot (\alpha_1 - \alpha_2) \quad (S1)$$

At the same time, in the frame of the model with independent stages, the conversion degree would be:

$$\frac{d\alpha}{dt} = \gamma A_1 e^{-E_{a1}/(RT)} \cdot (1 - \alpha_1) + (1 - \gamma) A_2 e^{-E_{a2}/(RT)} \cdot (1 - \alpha_2) \quad (S2)$$

It is clearly seen that the equations (S1) and (S2) in general yield different solutions. The reason for this is that the stages are not independent and are coupled via the $\alpha_1 - \alpha_2$, or, more generally, $f(\alpha_1, \alpha_2)$ term. Therefore, to properly separate the kinetic stages, we employed the isothermal kinetics.

4b. Formal kinetic models for the first stage of the TKX-50 decomposition

We started the fit of the first decomposition stage (Figure 3) from the simplest one-stage model using the most flexible Avrami-Erofeev (S3) and extended Prout-Tompkins (S4) forms. However, the performance of this model at both low and high conversion degree values turned out to be poor (Figure S6). Therefore, we considered next various two-stage formal kinetic schemes (*viz.*, consequent, parallel, independent reactions). The choice of the particular model was made on the basis of the Fisher statistics, the details are given in Table S2. The best fit to experimental data was found for a model of the Scheme S2 (the correlation coefficient 0.9996). The model commences with conversion of TKX-50 to an intermediate product (reaction R1), which is subsequently consumed in the reaction (R2).



Scheme S2.

The results of global fitting of activation energies, preexponential factors, and reaction model parameters (the so-called kinetic triplets) are given in Table S1. Note that the primary reaction (R1) (Scheme S2) is described by the Avrami–Erofeev nucleation-growth model [f]:

$$f(\alpha) = n \cdot (1 - \alpha) \cdot (-\ln(1 - \alpha))^{\frac{n-1}{n}} \quad (\text{S3})$$

The reaction order obtained from fitting ($n = 1.76$) is consistent with a model of two-dimensional growth of the nuclei with decelerating formation rate. At the same time, the kinetic model for the second stage of the Scheme S2 was described by the most general extended Prout-Tompkins form (usually denoted as Bna):

$$f(\alpha) = \alpha^m \cdot (1 - \alpha)^n \quad (\text{S4})$$

The particular values of the parameters obtained from fitting ($n = 0.4$, $m = 0.7$, Eq. S4, Table S1) render the model to be quite complex and not to correspond to a single elementary physical or chemical process.

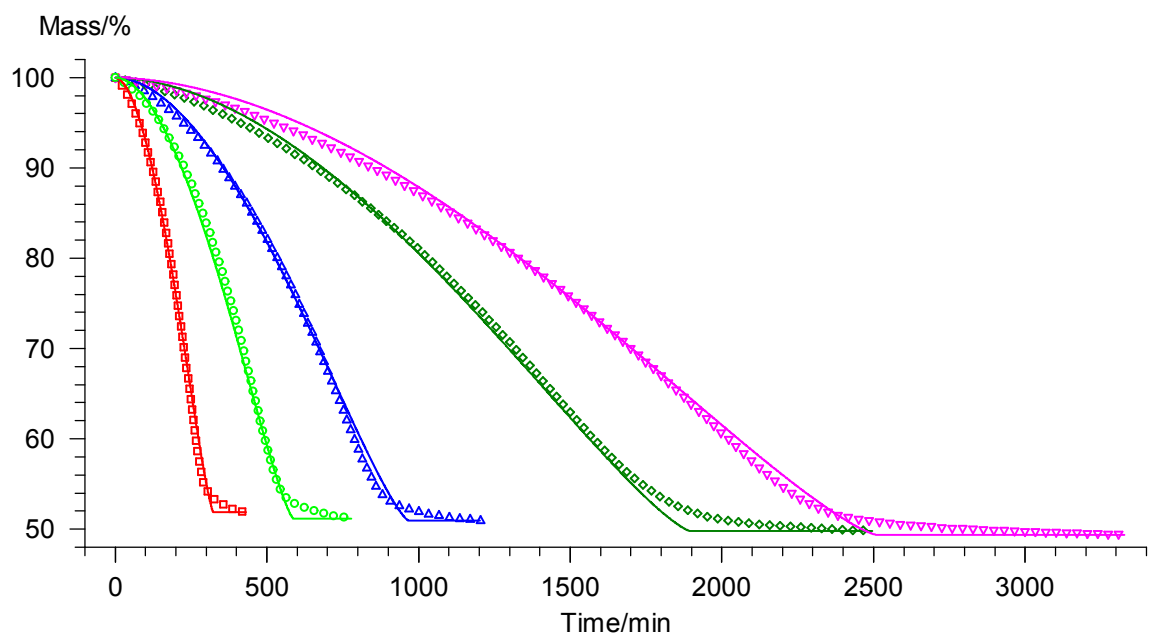


Figure S6. TGA isothermal data of TKX-50 decomposition (triangles, from right to left: 443, 446, 452, 457, and 463 K) and fit with the one-step reaction model (solid curves) of the extended Prout-Tompkins type (Bna , Eq. S4). Notable deviations are visible at low and high conversion degrees.

Table S1. The Formal Kinetic Parameters (Activation Energies, Preexponential Factors, and Reaction Models) for the Formal Kinetic Model of Scheme S2 (the Correlation Coefficient 0.9996).

Reactions ^a	R1	R2
$f(\alpha)$	$1.76 \cdot (1-\alpha) \cdot (-\ln(1-\alpha))^{0.43}$	$\alpha^{0.7} \cdot (1-\alpha)^{0.4}$
$\log(A / s^{-1})$	15.3	17.3
$E_a / \text{kJ mol}^{-1}$	171	185

^a The reactions are denoted in accordance with Scheme S2.

Table S2. Fischer criterion values for various models employed for fitting of the isothermal data.

F-TEST ON FIT-QUALITY

#	Code ^a	Fexp ^b	Fcrit(0.95) ^b	Type 1 ^c	Type 2 ^c	Scheme description
0	d:f;	1	1.03	An	Bna	Two stages, consecutive
1	d:f;	1.03	1.03	Bna	Bna	Two stages, consecutive
2	d:i;	1.26	1.03	Bna	Bna	Two stages, independent
3	d:p;	1.45	1.03	R2	Bna	Two stages, parallel, equal contribution
4	d:p;	1.46	1.03	Bna	Bna	Two stages, parallel, equal contribution
5	d:p;	1.46	1.03	R3	Bna	Two stages, parallel, equal contribution
6	d:i;	1.47	1.03	Fn	An	Two stages, independent
7	d:c;	1.48	1.03	Bna	An	Two stages, parallel, unequal contribution
8	d:f;	1.49	1.03	Bna	An	Two stages, consecutive
9	s:	1.69	1.03	Cn		One stage
10	d:f;	6.7	1.03	A2	An	Two stages, consecutive

F-TEST ON STEP-SIGNIFICANCE

#	Code ^a	Fexp ^b	Fcrit(0.95) ^b	f-act	Type 1 ^c	Type 2 ^c
0	s:	reference	15156	CnB		
1	d:f;	3489.49	8.55	15153	An	Bna

2	d:f;	2452.87	5.65	15152	Bna	Bna
3	d:i;	1027.62	4.38	15151	Bna	Bna
4	d:p;	1269.61	19.7	15154	R2	Bna
5	d:p;	600.22	5.65	15152	Bna	Bna
6	d:p;	1193.08	19.7	15154	R3	Bna
7	d:i;	749.44	8.55	15153	Fn	An
8	d:c;	424.36	4.38	15151	Bna	An
9	d:f;	499.54	5.65	15152	Bna	An
10	d:f;	-11332.7	358.47	15155	A2	An

^a Reaction scheme codes are given in accordance with [g], the last column contains the brief description of the particular schemes used.

^b Parameters of the Fisher statistics. The application of the Fischer criterion to the formal kinetics is described in [g,h]. In brief, the F_{exp} smaller than F_{crit} means that the model is statistically significant.

^c Reaction types are denoted in accordance with [g,i], the best model #0 comprises the consecutive Avrami-Erofeev (S3) and the extended Prout-Tompkins models (S4).

4c. The second stage of the TKX-50 decomposition: Isothermal vs. non-isothermal data

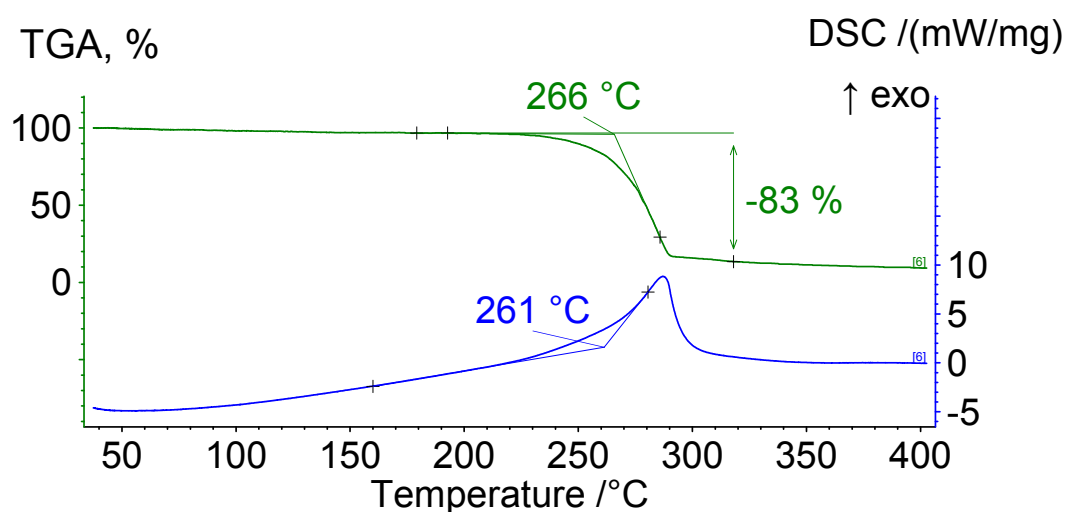


Figure S7. DSC and TGA curves for the decomposition of solid product (SP, Section 1) of the first stage under heating rate of 10 K min^{-1} . One main decomposition step was clearly observed with the mass loss close to the ABTOX content in the sample.

It is also instructive to compare the Friedman plots for isothermal and non-isothermal data (Figure S8). The isothermal activation energy (Figure S8, blue curve) is a monotonically decreasing function at $\alpha < 0.02$. This stage is followed by the two stages with approximately constant values of effective activation energy: $E_a \sim 180 \text{ kJ mol}^{-1}$ at $\alpha = 0.02-0.1$, and $E_a \sim 155 \text{ kJ mol}^{-1}$ at $\alpha > 0.3$ (Figure S8, blue curve). On the contrary, the non-isothermal DSC plot (Figure S8, red curve) exhibits a drastic increase of the effective activation energy at $\alpha < 0.3$ followed by the region of approximately constant activation energy $\sim 340 \text{ kJ mol}^{-1}$ in a range $0.3 < \alpha < 0.9$ (Figure S8, red curve). Note that the formal kinetic approach yields *the one-stage reaction* described by the three-dimensional diffusion model (Ginstling-Brounstein-type) with the kinetic parameters $E_a = 343 \pm 15 \text{ kJ mol}^{-1}$, $\log(A/s^{-1}) = 28.7 \pm 1.4$, $f(\alpha) = \frac{3}{2 \cdot (1/\sqrt[3]{1-\alpha} - 1)}$ (the experimental points along with fitting curves are shown in Figure S8). It is clearly seen that such values do not correspond to single-stage decomposition, and this simple description is not appropriate in the present case.

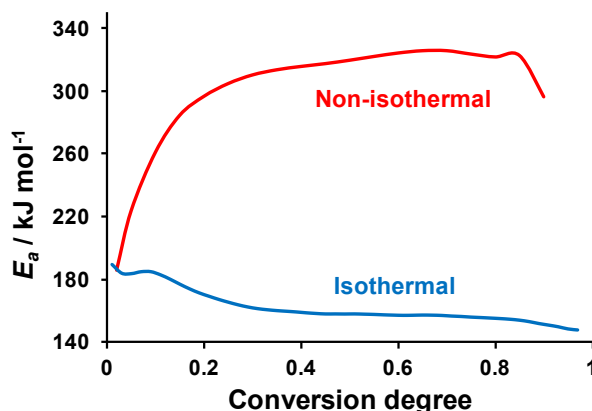


Figure S8. Isoconversional Friedman plots of effective activation energy against conversion degree for non-isothermal (red curve) and isothermal DSC (blue curve) of the solid product of the first decomposition stage.

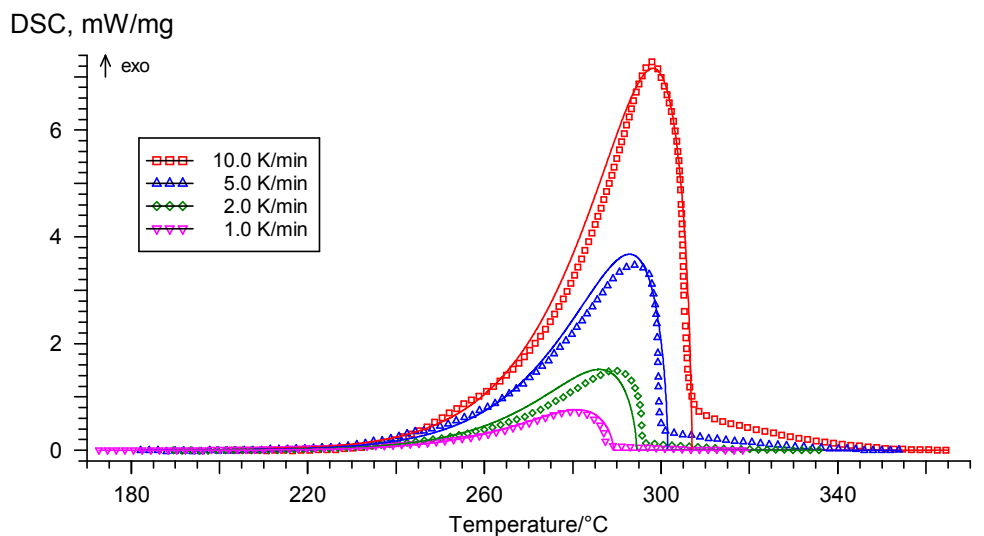
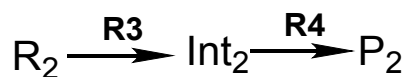


Figure S9. Second stage of the TKX-50 decomposition: experimental (points) and simulated (lines) DSC curves for non-isothermal ageing. The single-step 3D-diffusional kinetic model was applied.

Comparison of results obtained by isothermal heating with the non-isothermal one (Figure S8) reveals the initial decomposition process at $\alpha=0.02$ to be almost identical with the similar E_a values. However, in the case of non-isothermal heating (in a confined pan and at a higher heating rate), the overall decomposition process comprised of the two steps (Scheme S3) becomes complicated by diffusion, as evidenced by the reaction model.

4d. Formal kinetic models for second stage of the TKX-50 decomposition

Similarly to the case of the first stage of TKX-50 decomposition, the formal kinetic scheme was sequentially built by addition of the reaction steps in the flexible form of (S3) or (S4). The model comprised of the two subsequent reactions renders the best fit to these TGA curves (Scheme S3). The parameters of this model are given in Table S3 (cf. Table S2).



Scheme S3.

Table S3. The Formal Kinetic Parameters (Activation Energies, Preexponential Factors, and Reaction Models) for the Formal Kinetic Model of Scheme S3 (the Correlation Coefficient 0.9999).

Reactions ^a	R3	R4
$f(\alpha)$	$(1-\alpha)$	$\alpha^{0.33} \cdot (1-\alpha)^{0.4}$
$\log(A / s^{-1})$	16.1	12.1
$E_a / kJ mol^{-1}$	189	157

^a The reactions are denoted in accordance with Scheme S3.

4e. The third stage of the TKX-50 decomposition

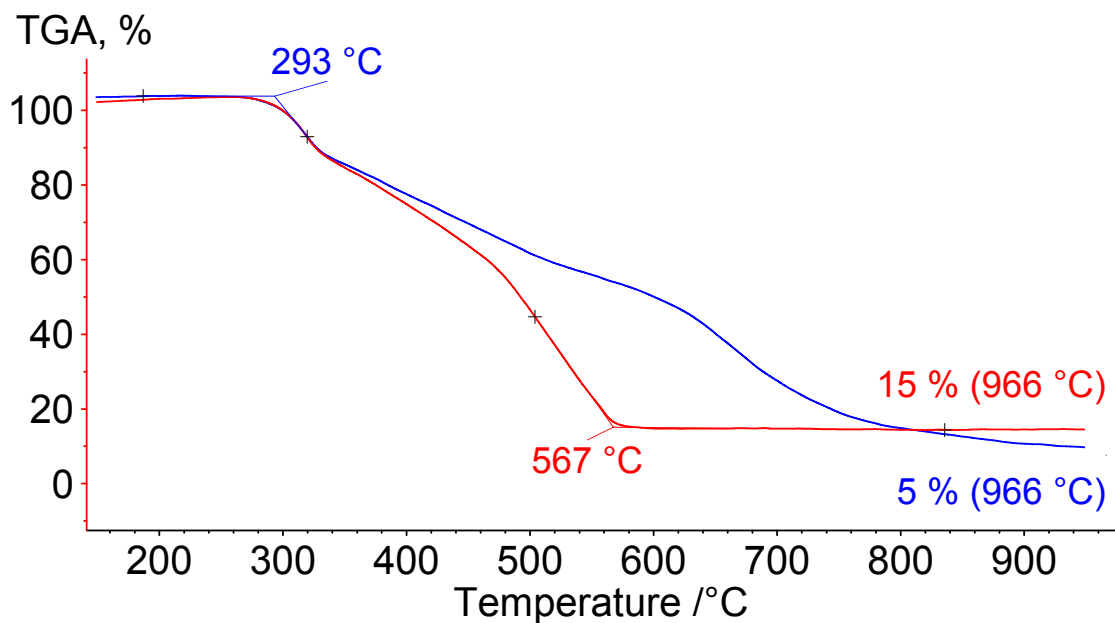


Figure S10. The third stage of TKX-50 thermolysis: decomposition of the product (FP) of the 2nd stage under inert (argon, blue curve) and oxidative (air, red curve) flow. The present data indicate the relatively high heat-resistance of this material.

[f] S. Vyazovkin, A. K. Burnham, J. M. Criado, L. A. Perez-Maqueda, C. Popescu and N. Sbirrazzuoli, *Thermochim. Acta*, 2011, **520**, 1-19.

[g] NETZSCH Thermokinetics Software 3.1, NETZSCH Corporation: Selb, Germany, 2014.

[h] Opfermann, J., Kinetic analysis using multivariate non-linear regression - I. Basic concepts. *J. Therm. Anal. Calorim.* 2000, **60**, 641-658.

[i] Sharp, J. H.; Brindley, G. W.; Achar, B. N. N., Numerical Data for Some Commonly Used Solid State Reaction Equations. *J. Am. Ceram. Soc.* 1966, **49**, 379-382.

5. Analysis of the evolved gases by IR spectroscopy

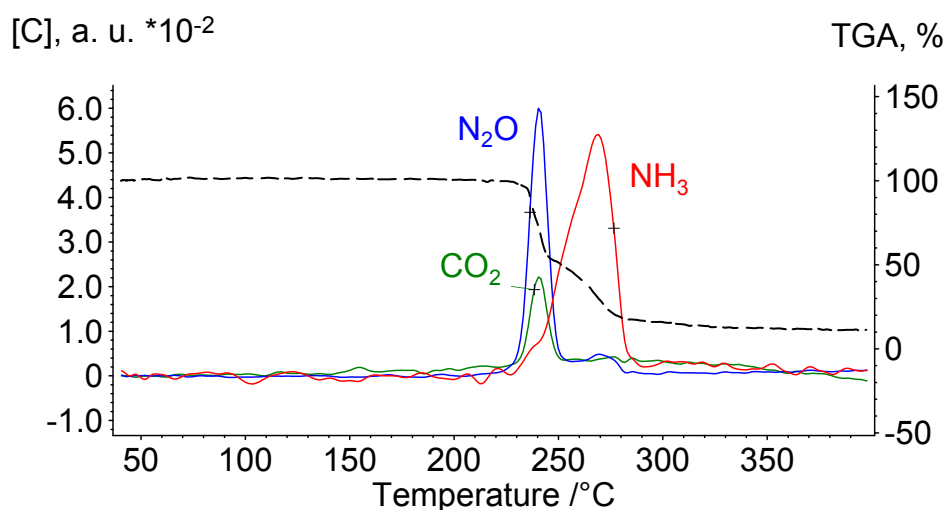


Figure S11. Evolution of IR-active gaseous products of TKX-50 decomposition under linear heating of 10 K/min. The concentrations of species are presented relative to that of CO₂, the IR absorbance values were taken from [j].

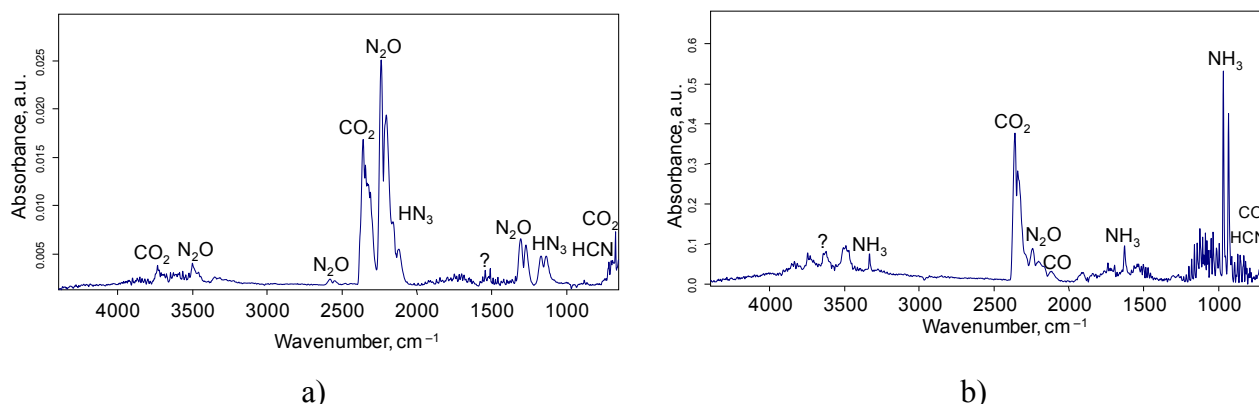


Figure S12. IR-spectra of gaseous decomposition products during: (a) 1st stage of TKX-50 decomposition, isothermal run at 465 K; (b) 2nd stage of TKX-50 decomposition, isothermal run at 529 K.

[j] Brill T. B.; Arisawa H.; Brush P. J.; Gongwer P. E.; Williams G. K., Surface Chemistry of Burning Explosives and Propellants. *J. Phys. Chem.* 1995, **99**, 1384-1392.

6. Accelerating rate calorimetry: experiment and modeling

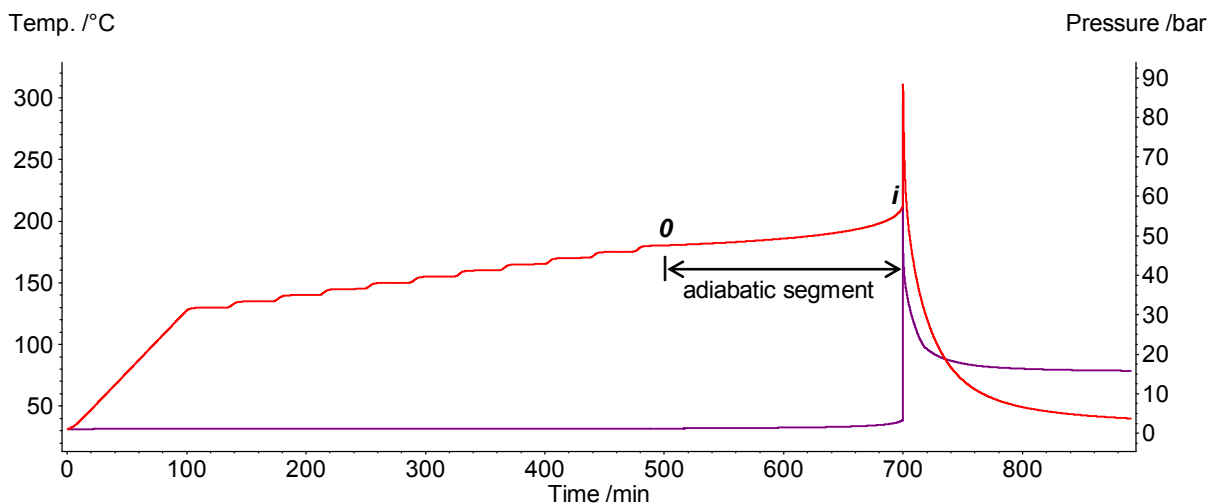


Figure S13. ARC run #2 data: temperature (red curve) and pressure (violet curve) versus time. The point “o” indicate the detected onset of the self-heating, while the point “i” corresponds to ignition of the sample.

Table S4. Comparison of the Kinetic Predictions with ARC Data: Initial Self-Heating Rate (SHR_0) and Time to Maximum Rate (TMR_{ad}).

Set ^a	Experimental details	$\Phi=15.1$		$\Phi=19.5$	
		$\Delta SHR_0, \%$	$\Delta TMR_{ad}, \%$	$\Delta SHR_0, \%$	$\Delta TMR_{ad}, \%$
IFK-2CP	Isotherms, m=50 mg, $T=443-463$ K, $\alpha_{max}=0,49$	-45	58	-47	52
IFM		-28	3	-35	12
IVM		-30	4	-37	14
NKM03	Non-isothermal m=0.3 mg, $\beta=2-40$ K min ⁻¹	186	-44	137	-30
NFM03		124	-59	178	-65
NVM03		71	-53	133	-60
NKM03-L	Non-isothermal m=0.3 mg, $\beta=2-10$ K min ⁻¹	278	-56	207	-44
NFM03-L		85	-52	116	-56
NVM03-L		56	-47	93	-53
NKM1	Non-isothermal m=1 mg, $\beta=1-20$ K min ⁻¹	430	-59	293	-45
NFM1		402	-73	382	-75

NVM1			265	-66	288	-70
NKM1-L	Non-isothermal $\beta=0.5-2 \text{ K min}^{-1}$	m=1 mg,	643	-62	299	-63
NFM1-L			988	-85	566	-94
NVM1-L			965	-85	565	-91
NKM[k] ^b	Non-isothermal $\beta=1-20 \text{ K min}^{-1}$	m=1 mg,	639	-70	394	-58
NFK [k] ^c	Non-isothermal $\beta=1-20 \text{ K min}^{-1}$	m=0.5 mg,	988	-93	569	-75
NKM[l] ^d	Non-isothermal $\beta=5-20 \text{ K min}^{-1}$	m=1 mg,	1000	-92	736	-92
NKM[m] ^e	Non-isothermal $\beta=2-32 \text{ K min}^{-1}$	mass not reported,	498	-67	344	-55
IFK-2P[m] ^f	Isotherms, mass not reported; Full curves 463, 468, 473 K, partial conversion 443, 453, 458 K		35	-57	23	-54

Notes:

^a First letter “I” denotes isothermal, “N” – non-isothermal; the next two letters: “FK” – formal kinetic, “FM” – Friedman isoconversional, “VM” – Vyazovkin isoconversional, “KM” – Kissinger model-free method; “2P” – the model with two parallel steps; “2CP” – the model with 2 consecutive stages.

^b Kinetic parameters: $E_a=143.2 \text{ kJ mol}^{-1}$, $\log(A/s^{-1})=12.299$.

^c Kinetic parameters for one-step model: $E_a=169.5 \text{ kJ mol}^{-1}$, $\log(A/s^{-1})=15.588$, $n=1$, $m=0$.

^d Kinetic parameters: $E_a=237.59 \text{ kJ mol}^{-1}$, $\log(A/s^{-1})=23.89$.

^e Kinetic parameters: $E_a=156.64 \text{ kJ mol}^{-1}$, $\log(A/s^{-1})=13.7$.

^f Kinetic parameters for the model with two parallel reactions, the first: $E_a=166.86 \text{ kJ mol}^{-1}$, $\log(A/s^{-1})=13.774$, $n=1$, $m=0$; the second: $E_a=190.22 \text{ kJ mol}^{-1}$, $\log(A/s^{-1})=18.068$, $n=1$, $m=1$.

[k] Fischer, D.; Klapotke, T. M.; Musanic, S. M.; Stierstorfer, J.; Suceca, M. In TKX-50, Proceedings of New Trends in Research of Energetic Materials, Czech Republic, 2013; pp 566-577.

[l] Huang, H. F.; Shi, Y. M.; Yang, J., Thermal characterization of the promising energetic material TKX-50. *J. Therm. Anal. Calorim.* 2015, **121**, 705-709.

[m] Sinditskii, V. P.; Filatov, S. A.; Kolesov, V. I.; Kapranov, K. O.; Asachenko, A. F.; Nechaev, M. S.; Lunin, V. V.; Shishov, N. I., Combustion behavior and physico-chemical properties of dihydroxylammonium 5,5'-bistetrazole-1,1'-diolate (TKX-50). *Thermochim. Acta* 2015, **614**, 85-92.

7. Recommended kinetic parameters for first stage of TKX-50 decomposition

Table S5. Isoconversional Friedman Kinetic Parameters Yielding the Best Fit of the TKX-50 Decomposition Under Adiabatic Conditions (Figure 10 and Table S2).

α	$E_a / \text{kJ mol}^{-1}$	$\Delta E_a / \text{kJ mol}^{-1}$	$\ln\{(A/s^{-1}) \cdot f(\alpha)\}$	R^2	α	$E_a / \text{kJ mol}^{-1}$	$\Delta E_a / \text{kJ mol}^{-1}$	$\ln\{(A/s^{-1}) \cdot f(\alpha)\}$	R^2
0.005	159.6	7.2	30.2	0.994	0.250	185.7	2.1	38.7	1.000
0.015	169.1	4.8	33.1	0.998	0.260	185.8	2.1	38.8	1.000
0.025	171.1	4.1	33.8	0.998	0.270	185.8	2.2	38.8	1.000
0.034	172.2	3.4	34.2	0.999	0.279	186.0	2.5	38.9	0.999
0.044	174.0	2.7	34.8	0.999	0.289	186.1	2.7	38.9	0.999
0.054	175.9	2.3	35.4	0.999	0.299	186.3	3.0	39.0	0.999
0.064	177.3	2.1	35.8	1.000	0.309	186.2	3.2	39.0	0.999
0.074	178.2	1.9	36.1	1.000	0.319	186.2	3.4	39.0	0.999
0.083	178.9	1.8	36.4	1.000	0.328	186.1	3.8	39.0	0.999
0.093	180.0	1.6	36.7	1.000	0.338	186.2	4.1	39.0	0.999
0.103	180.8	1.6	37.0	1.000	0.348	186.3	4.7	39.0	0.998
0.113	181.5	1.5	37.2	1.000	0.358	186.4	5.0	39.1	0.998
0.123	182.3	1.4	37.5	1.000	0.368	186.7	5.9	39.1	0.997
0.132	182.8	1.3	37.6	1.000	0.377	187.2	6.4	39.2	0.996
0.142	183.0	1.2	37.7	1.000	0.387	187.5	7.1	39.3	0.996
0.152	183.7	1.5	37.9	1.000	0.397	188.3	8.0	39.5	0.995
0.162	183.4	1.2	37.9	1.000	0.407	188.7	9.1	39.6	0.993
0.172	183.8	1.3	38.0	1.000	0.417	189.0	10.6	39.6	0.991
0.181	184.1	1.2	38.2	1.000	0.426	188.3	11.4	39.4	0.989
0.191	184.7	1.6	38.3	1.000	0.436	186.6	12.1	38.8	0.988
0.201	184.7	1.4	38.4	1.000	0.446	182.3	12.4	37.5	0.986
0.211	185.0	1.7	38.5	1.000	0.456	172.9	11.3	34.8	0.987
0.221	185.1	1.8	38.5	1.000	0.466	151.8	9.4	28.7	0.989
0.230	185.6	1.8	38.7	1.000	0.475	146.5	11.9	26.5	0.981
0.240	185.7	2.1	38.7	1.000	0.485	187.1	12.3	36.3	0.987